



CHORUS

This is the accepted manuscript made available via CHORUS. The article has been published as:

Collective excitation of a trapped Bose-Einstein condensate with spin-orbit coupling

Li Chen, Han Pu, Zeng-Qiang Yu, and Yunbo Zhang

Phys. Rev. A **95**, 033616 — Published 15 March 2017

DOI: [10.1103/PhysRevA.95.033616](https://doi.org/10.1103/PhysRevA.95.033616)

Collective excitation of a trapped Bose-Einstein condensate with spin-orbit coupling

Li Chen^{1,2}, Han Pu^{2,3,*}, Zeng-Qiang Yu¹, and Yunbo Zhang^{1†}

¹*Institute of Theoretical Physics, Shanxi University, Taiyuan, Shanxi 030006, P. R. China*

²*Department of Physics and Astronomy, and Rice Center for Quantum Materials, Rice University, Houston, TX 77005, USA*

³*Center for Cold Atom Physics, Chinese Academy of Sciences, Wuhan 430071, China*

We investigate the collective excitations of a Raman-induced spin-orbit coupled Bose-Einstein condensate confined in a quasi one-dimension harmonic trap using the Bogoliubov method. By tuning the Raman coupling strength, three phases of the system can be identified. By calculating the transition strength, we are able to classify various excitation modes that are experimentally relevant. We show that the three quantum phases possess distinct features in their collective excitation properties. In particular, the spin dipole and the spin breathing modes can be used to clearly map out the phase boundaries. We confirm these predictions by direct numerical simulations of the quench dynamics that excites the relevant collective modes.

PACS numbers: 03.75.Mn, 37.10.Vz, 67.85.De

I. INTRODUCTION

In recent years, an important breakthrough in cold atom physics is the realization of spin-orbit (SO) coupling [1–5]. The SO coupled Bose gases, which has no analog in conventional solid materials which deal with fermionic systems, present rich many-body quantum phases such as stripe phase [6–10] and skyrmion lattices [11]. However, despite of the tremendous attention they have attracted, direct evidences of these exotic phases are still lacking [12].

The main purpose of the present work is to show that different phases of an SO coupled Bose-Einstein condensate (BEC) features distinctive collective excitations, which can therefore be used to distinguish various phases. We will focus on the most commonly achieved system: a spin-1/2 BEC confined in a harmonic trap and subject to the Raman-induced equal-weight Rashba Dresselhaus SO coupling. Some of the nontrivial properties of the collective excitation of such a system has already been explored. For example, the softening of roton-like gap as well as the sound velocity are experimentally measured [13, 14], and the deviation of the dipole oscillation frequency away from the trapping frequency has also been observed [15–18]. This deviation is a distinct feature of the SO coupling. Here we examine the Bogoliubov spectrum of the system, develop a technique to classify different types of collective excitations across the whole phase diagram, and show how they can help us identify different phases.

II. MODEL

We consider an effectively one-dimension system by assuming that the Raman beams propagate along the x -

axis with vanishing two-photon detuning, and the BEC is tightly confined along the y - and the z -axis. Under the mean-field framework, the BEC is governed by the following Gross-Pitaevskii (GP) equation: (we set $\hbar = M = 1$ with M being the atomic mass)

$$i\partial\Psi(x,t)/\partial t = (H_0 + \mathcal{G})\Psi(x,t), \quad (1)$$

where we have labeled the two spin components as \uparrow and \downarrow , $\Psi = (\psi_\uparrow, \psi_\downarrow)^T$ is the spinor wave function which is normalized such that $\int dx |\Psi|^2 = N$ with N being the total atom number,

$$H_0 = k_x^2/2 - k_L k_x \sigma_z + \Omega \sigma_x/2 + V(x), \quad (2)$$

is the single-particle Hamiltonian where k_L denotes the Raman recoil momentum, $V = \omega_x^2 x^2/2$ represents the external harmonic potential with ω_x being the trapping frequency, and Ω denotes the Raman coupling strength. In Eq. (1), $\mathcal{G} = \text{diag}(g_{\uparrow\uparrow}|\psi_\uparrow|^2 + g_{\uparrow\downarrow}|\psi_\downarrow|^2, g_{\downarrow\downarrow}|\psi_\downarrow|^2 + g_{\downarrow\uparrow}|\psi_\uparrow|^2)$ characterizes the two-body interaction. Here we assume that the interaction is repulsive such that all interaction strengths $g_{\sigma\sigma'} > 0$. Moreover, for simplicity, we will take the intra-spin interaction to be equal, i.e., $g_{\uparrow\uparrow} = g_{\downarrow\downarrow} = g$.

For a homogeneous system, the single-particle ground state is doubly degenerate, occurring at $k_x = \pm k_0 = \pm\sqrt{k_L^2 - \Omega^2/4k_L^2}$ when $\Omega < 4E_L$, and for $\Omega > 4E_L$, the two degenerate states merge into a single one with $k_0 = 0$. Here, $E_L \equiv k_L^2/2$ is the recoil energy. This leads to three mean-field BEC phases: For $\Omega > 4E_L$, all atoms condense to the zero momentum state and hence this phase is termed as zero-momentum phase (ZM); for $\Omega < 4E_L$, depending on the interaction strength, we may have all the atoms condense to one of the degenerate single-particle ground states and we have the plane-wave phase (PW); or the atoms can condense to an equal-weight superposition of the two degenerate single-particle ground states and we have the stripe phase (ST), as both spin components exhibit density stripes. In the presence of a weak harmonic trap, even though momentum is no longer a good

*Electronic address: hpu@rice.edu

†Electronic address: ybzhang@sxu.edu.cn

quantum number, the analog of all the three phases can still be easily identified, and the main effects of the trap is to provide an overall envelop for the atomic density and the boundaries between different phases are shifted [19].

We obtain the condensate ground state wave function Ψ_0 by numerically propagating the GP equation in imaginary time [20]. The numerical results are in very good agreement with the following ansatz [7]

$$\Psi_0 \approx \left[C_1 \begin{pmatrix} \cos \theta \\ -\sin \theta \end{pmatrix} e^{ik_0 x} + C_2 \begin{pmatrix} \sin \theta \\ -\cos \theta \end{pmatrix} e^{-ik_0 x} \right] G. \quad (3)$$

Here, $G(x) = e^{-x^2/2w^2}$ is a Gaussian envelop accounting for the trap confinement with w being the envelop width, C_1 and C_2 are amplitudes for the two plane waves with momentum $\pm k_0$, respectively. The three phases can then be characterized as follows. For the ST phase, we have $C_1 = C_2$ and $k_0 \neq 0$; for the PW phase, $C_1 = 0$ or $C_2 = 0$ and $k_0 \neq 0$; for the ZM phase, $C_1 = C_2$ and $k_0 = 0$.

Different phases can be accessed by tuning the Raman coupling strength Ω . For strong inter-spin interaction with $g_{\uparrow\downarrow} \geq g$, the system is in the PW (ZM) phase if $\Omega < \Omega_C^{P-Z}$ ($\Omega > \Omega_C^{P-Z}$) and the ST phase is absent. The critical value $\Omega_C^{P-Z} = 4E_L$ for a homogeneous system, and is slightly down shifted by the trap [19]. For weaker inter-spin interaction with $g_{\uparrow\downarrow} < g$, the ST phase is also present at small Raman coupling strength $\Omega < \Omega_C^{S-P}$, the PW phase exists when $\Omega_C^{S-P} < \Omega < \Omega_C^{P-Z}$, and the ZM phase remains at large Raman coupling strength when $\Omega > \Omega_C^{P-Z}$. Previous studies have shown that the ST to PW transition at Ω_C^{S-P} is of first-order, whereas the PW to ZM transition at Ω_C^{P-Z} is of second-order [7].

In our calculation, we will take $g_{\uparrow\downarrow} = 0.7g$. As in this case, all three phases are present. In addition, we will take the atom number to be $N = 2000$, and consider a relatively weak but realistic trap with $\omega_x = 0.02E_L$. For this set of parameters, the two critical Raman coupling strengths are $\Omega_C^{S-P} \approx 2E_L$ and $\Omega_C^{P-Z} \approx 4E_L$.

III. BOGOLIUBOV SPECTRA

We study the collective excitation of the system using the method of Bogoliubov theory [21]. To this end, we construct the following wave function which includes small fluctuations above the ground state:

$$\Psi = e^{-i\mu t} [\Psi_0 + \mathbf{u}_n(x) e^{-i\omega_n t} + \mathbf{v}_n(x) e^{i\omega_n t}], \quad (4)$$

where μ is the chemical potential, $\mathbf{u}_n = (u_{n\uparrow}, u_{n\downarrow})^T$ and $\mathbf{v}_n = (v_{n\uparrow}, v_{n\downarrow})^T$, satisfying the normalization condition $\int dx (|\mathbf{u}_n|^2 - |\mathbf{v}_n|^2) \equiv 1$, are the Bogoliubov quasi-particle amplitudes. By inserting Ψ into GP Eq. (1) and keeping the fluctuation terms to linear order, the Bogoliubov equations are obtained (see Appendix). We

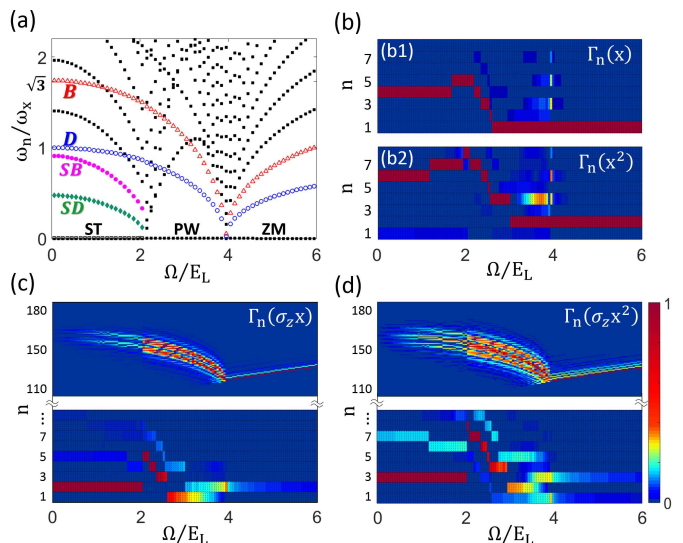


FIG. 1: (Color online) (a) Bogoliubov spectrum as functions of the Raman coupling strength Ω . Hollow circles and triangles denote the frequency of the dipole (D) and the breathing (B) mode, respectively; while solid diamonds and disks correspond to the spin dipole (SD) and the spin breathing (SB) frequencies. Furthermore, black hollow squares label the near zero-energy mode in the ST phase. (b1), (b2), (c) and (d) correspond to the normalized transition strength Γ_n of the dipole, the breathing, the spin dipole and the spin breathing modes, respectively. (b)-(d) share the same colormap at the right side of (d). In our calculations, we take $g_{\uparrow\downarrow} = 0.7g$ where g is calculated with the ^{87}Rb BEC in a condition that $\omega_x = 2\pi \times 45$ Hz, $a = 101.8a_B$ with a_B being the Bohr radius, and total atom number $N = 2000$.

solve the Bogoliubov equations numerically to find quasi-particle excitation frequency ω_n , as well as \mathbf{u}_n and \mathbf{v}_n .

Figure 1(a) shows a typical Bogoliubov spectrum ω_n as a function of the Raman coupling strength Ω , with all other parameters fixed. First one can see that for any Ω , there exists a zero mode with $\omega_0 = 0$, which corresponds to the ground state itself. In the thermodynamic limit, this zero mode corresponds to the Goldstone mode resulting from the spontaneous breaking of the U(1) gauge symmetry. At small Ω when the system is in the ST phase, there exists an additional low-lying mode (marked with black hollow squares) whose frequency is very close to zero. From the examination of the quasi-particle amplitudes, we find that, for this mode, $-\mathbf{v}^* \approx \mathbf{u} = \Psi_0^-$ where Ψ_0^- is approximately given by Eq. (3) with $C_1 = -C_2$. In the thermodynamic limit, the frequency of this mode will also vanish [8, 9], and it corresponds to the second Goldstone mode resulting from the spontaneous breaking of the translational symmetry which is unique for the ST phase [22]. These zero modes also serve as a self-consistency check for the accuracy of our numerical calculation.

Another rather apparent feature is that the spectrum exhibits mode softening near the two critical Raman coupling strength where the system changes from one phase

to another. It is therefore important to classify the excitation modes. This can be achieved by examining the corresponding quasi-particle amplitudes \mathbf{u}_n and \mathbf{v}_n . Specifically, we design the following method for mode identification. First we identify the operator \hat{O} that excite a specific mode. We will focus on the following modes: dipole, breathing, spin dipole, and spin breathing modes, with the corresponding excitation operators x , x^2 , $\sigma_z x$, and $\sigma_z x^2$, respectively [23–27]. We then calculate the normalized transition strength as follows (for details, see Appendix):

$$\Gamma_n(\hat{O}) = \frac{|\langle n | \hat{O} | 0 \rangle|}{\max \left[\left[|\langle n | \hat{O} | 0 \rangle|_{n=1}^\infty \right] \right]}. \quad (5)$$

Here $|0\rangle$ denotes the ground state, and $|n\rangle$ is the n th quasi-particle mode in ascending order. If a mode has $\Gamma_n(\hat{O})$ close to 1, then it reflects the main excitation features of the perturbation \hat{O} , and we classify this mode accordingly. Examples of $\Gamma_n(\hat{O})$ are presented in Fig. 1(b)-(d), which help us to identify those modes labeled in Fig. 1(a). In the following, we present a more detailed discussion of these modes.

IV. DIPOLE AND BREATHING MODES

A dominant dipole and a dominant breathing mode are present in all three phases. Their normalized transition strengths are plotted in Fig. 1(b1) and (b2), respectively. At $\Omega = 0$, i.e., in the absence of the SO coupling, their frequencies are given by: $\omega_D = \omega_x$ [28] and $\omega_B = \sqrt{3}\omega_x$ [24, 25], in full agreement with our numerical results. A common feature of these two modes is that they become soft with frequency tending to zero at $\Omega = \Omega_C^{P-Z}$, i.e., at the phase boundary between the PW and the ZM phases. However, at the other phase boundary between the ST and the PW phase, these two modes do not exhibit any special features. The softening of the dipole mode at Ω_C^{P-Z} has been studied by Li *et al.* [17]. Using a sum rule approach, they have shown that near $\Omega = \Omega_C^{P-Z}$, the dipole mode frequency $\omega_D \propto 1/\sqrt{\chi}$ where χ is the spin polarizability which diverges at $\Omega = \Omega_C^{P-Z}$. Alternatively, as pointed out in the Refs. [13] and [18], the low-lying collective modes can be described by a hydrodynamic equation with an effective trapping frequency $\sqrt{m/m^*}\omega_x$, and the divergence of the effective mass m^* at critical point Ω_C^{P-Z} is also able to explain the softening behavior in this region. In 2012, Zhang and coworkers [16] experimentally measured the dipole oscillation frequency of an SO coupled Rb condensate. They indeed found evidence of the mode softening near the phase boundary. However, the frequency never reaches zero. In fact, the dipole oscillation became quite complicated near Ω_C^{P-Z} and could not be fitted by a single frequency. They attributed these features to the

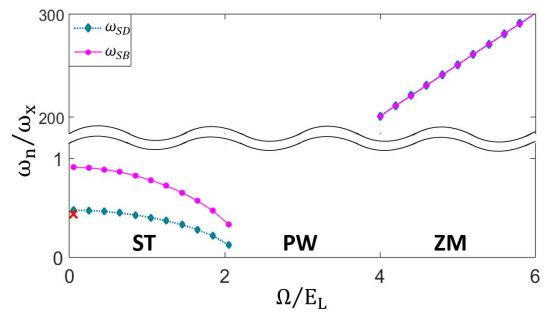


FIG. 2: (Color online) The spin dipole (SD) and the spin breathing (SB) mode frequency as functions of the Raman coupling strength Ω . These two modes are not well defined in the PW phase. Other parameters are the same as in Fig. 1.

nonlinear effects [16, 17]. From our plot of the normalized transition strength in Fig. 1(b1), we find that, near Ω_C^{P-Z} , there exist several low-lying modes with significant dipole transition strengths, which can be excited simultaneously in the experiment. This can explain the complicated behavior of the dipole oscillation near Ω_C^{P-Z} observed in the experiment.

As we have mentioned, the breathing mode exhibits a very similar behavior as the dipole mode and vanishes at $\Omega = \Omega_C^{P-Z}$. Furthermore, there also exist several low-lying modes with significant breathing transition strengths, as can be seen in Fig. 1(b2). Hence we expect similar complicated behavior near the phase boundary, just as in the case of the dipole mode.

V. SPIN DIPOLE AND SPIN BREATHING MODES

The spin dipole (SD) mode operator is $x\sigma_z$. In practice, this mode can be excited by adding a spin-dependent magnetic gradient. The normalized transition strength $\Gamma(x\sigma_z)$ is plotted in Fig. 1(c), and the mode frequency ω_{SD} across the whole phase diagram is plotted in Fig. 2 (diamonds with dotted line), from which we observe the following: In the ST phase, there is a dominant low-lying SD mode. Its frequency decreases as Ω increases, but remains finite at the ST/PW phase boundary. At $\Omega = 0$, our system reduces to a binary condensate without SO coupling. Based on the sum rule and the local density approximation, the SD frequency for such a system is given by [26]:

$$\omega_{SD} = \sqrt{\frac{g - g_{\uparrow\downarrow}}{g + g_{\uparrow\downarrow}}} \omega_x,$$

which leads to $\omega_{SD} \approx 0.42\omega_x$ when plugging in the parameters used in our calculation. This is plotted as the red cross in Fig. 2, and is in good agreement with our numerical result. In the PW phase, there is no single dominant spin dipole mode. This is particularly true away from the ST/PW phase boundary. In the ZM phase,

there is a dominant SD mode, but its frequency is much higher than the one in the ST phase. Further examination shows that the SD frequency in this regime is very close to the Raman coupling strength Ω (see discussion below).

To gain further insights of the spin dipole mode, we carry out a direct numerical simulation of the condensate dynamics. We add a small spin-dependent magnetic gradient in the system, which introduces an additional term $-\delta\sigma_z x$ in the Hamiltonian. The ground state density profiles without and with the magnetic gradient are plotted in the upper and lower rows in Fig. 3(a), respectively. In the absence of the gradient, the PW phase possesses a finite magnetization and the density profiles for the two spin components are different. By contrast, both the ST and the ZM phases are unmagnetized with identical density profiles in the two spin components. The characteristic density modulations in the ST phase are, however, difficult to observe in practice, as the spatial period of these oscillation is on the order of optical wavelength, which is far below the resolution of a typical imaging system. This poses as a great challenge for the direct observation of the ST phase [12]. In the presence of the gradient, the center-of-mass of the two spin components are displaced in opposite directions. In the ST phase, the density oscillations are still present and such oscillations in the two spin components remain in phase. The magnetic gradient has the most dramatic effect on the PW state: the overall magnetization is now zero but the two spin components are separated in space with a rather sharp domain wall between them.

To study the spin dipole dynamics, we prepare the system in the ground state in the presence of the magnetic gradient, and then suddenly quench the magnetic gradient to zero at $t = 0$ and follow the dynamics of the system by solving the time-dependent GP equation in real time [29]. We define the displacement between the two spin components as $\mathcal{D}(t) = \langle x_\uparrow(t) \rangle - \langle x_\downarrow(t) \rangle$ with $\langle x_\sigma \rangle = \int dx |\Psi_\sigma(x)|^2 x$. Typical dynamics of $\mathcal{D}(t)$ for the three phases are plotted in Fig. 2(b)-(d), which we describe below.

(1) For the ST phase depicted in Fig. 3(b), $\mathcal{D}(t)$ oscillates roughly sinusoidally around zero, with an oscillation frequency matching very well with the one obtained from the Bogoliubov calculation ω_{SD} . Furthermore, during the time evolution, the density modulations in the two spin components remain ‘phase locked’. We found that the dynamics can be accurately reproduced using the Bogoliubov approach, under which the time-dependent condensate wave function is given by Eq. (4). For the SD mode, we found that $\mathbf{v} \approx 0$ and $\mathbf{u} \approx \eta x \Psi_0^- / w$ where η characterizes a small excitation amplitude. From these, the density profile for each spin component can be calculated

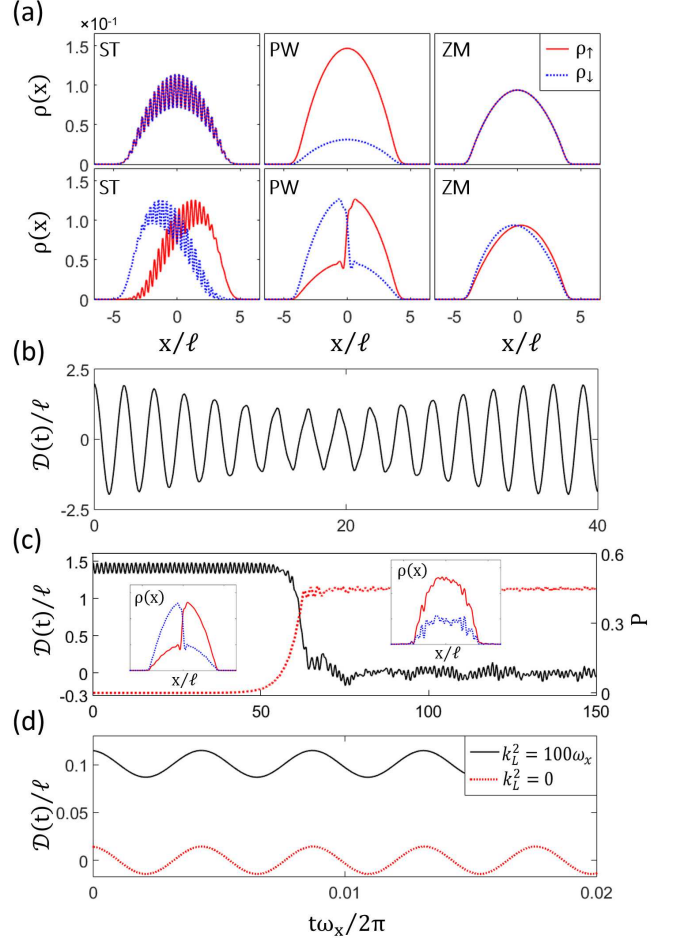


FIG. 3: (Color online) (a) Upper row: ground state density profiles in three phases, where $\ell = \omega_x^{-1/2}$ is the harmonic oscillator length. Lower row: density profiles in the presence of a magnetic gradient with $d = \omega_x^2 \ell / 4$. In the calculation, we take $\Omega = E_L, 3.5E_L$ and $4.5E_L$ to represent the ST, the PW and the ZM phase, respectively. The evolution of the spin separation $\mathcal{D}(t)$ after the sudden quench of the magnetic gradient for the three phases are illustrated in (b), (c) and (d), respectively. (b) Evolution of $\mathcal{D}(t)$ in the ST phase. (c) Evolution of $\mathcal{D}(t)$ (black solid line) and polarization P (red dotted line) in the PW phase. The two insets show the typical density profiles before and after the jump which occurs around $t = 60$ trap periods. (d) Evolution of $\mathcal{D}(t)$ in the ZM phase, with (black solid line) and without (red dotted line) the SO coupling, respectively. Other parameters are the same as in Fig. 1.

as

$$\begin{aligned} \rho_\sigma(t) &= |\Psi_{0,\sigma}(x) + u_\sigma(x) e^{-i\omega_{SD}t}|^2 \\ &\sim \left[\sin 2\theta \left(\cos 2k_0 x + \frac{2\eta x}{w} \sin 2k_0 x \sin \omega_{SD}t \right) \right. \\ &\quad \left. + \left(1 \pm \frac{2\eta x}{w} \cos 2\theta \cos \omega_{SD}t \right) + O(\eta^2) \right] G^2, \end{aligned} \quad (6)$$

where \pm corresponds to $\sigma = \uparrow$ and \downarrow , respectively. Here, we have ignored a global normalization constant in

Eq. (6). One can see that the first term in the square bracket ensures that the spatial density modulations are in phase for the two spin components.

(2) For the PW phase depicted in Fig. 3(c), the response of the system is rather nonlinear. In the beginning of the evolution, $\mathcal{D}(t)$ carries out small-amplitude oscillations around the initial value, indicating the presence of a stiff domain wall. At $t \approx 60$ trap periods, the domain wall collapses and the systems jumps to a situation close to the ground state in the absence of the gradient, accompanied by a jump of the overall magnetization P from zero to a finite value. Typical density profiles before and after this jump are shown as the two insets in Fig. 3(c). This nonlinear behavior is consistent with the Bogoliubov result we obtained earlier. In particular, Fig. 1(c) shows that there are a large number of quasi-particle modes with significant SD transition strength in the PW phase. The dynamical behavior may be regarded as resulting from the nonlinear mode coupling among these modes.

(3) Finally, for the ZM phase depicted in Fig. 3(d), $\mathcal{D}(t)$ oscillates sinusoidally with a frequency slightly above Ω , again in full agreement with the Bogoliubov result. Furthermore, $\mathcal{D}(t)$ never changes sign for the parameters we used in our simulation (if we use a large enough Ω , $\mathcal{D}(t)$ may change sign, but the oscillation would remain asymmetric about zero). In comparison, we also simulated the spin dipole dynamics of a coherently coupled two-component BEC without SO coupling [27], by taking $k_L = 0$ in Hamiltonian (2), shown as the red dotted line in Fig. 3(d). The main difference with and without the SO coupling is that, in the latter case, $\mathcal{D}(t)$ oscillates symmetrically about zero. This difference can be understood in a simple way. The Raman coupling term in Hamiltonian (2) may be regarded as an effective uniform transverse magnetic field along the x -axis. In the absence of the magnetic gradient, the atoms are therefore spin polarized along the x -axis. The weak magnetic gradient tips the atomic spin slightly away from the x -axis. After the quench of the magnetic gradient and in the absence of the SO coupling, the atomic spin precesses around the effective transverse magnetic field, with the Larmor frequency given by Ω . In one period, the spin rotates about the x -axis in a full circle, rendering $\mathcal{D}(t)$ to oscillate about zero symmetrically. By contrast, in the presence of the SO coupling, the SO coupling term may be regarded as an effective momentum-dependent longitudinal magnetic field along the z -axis, which tends to maintain the value of σ_z . Hence the spin flip becomes incomplete and $\mathcal{D}(t)$ tends to maintain its original sign.

Finally, let us briefly discuss the spin breathing (SB) mode with the corresponding perturbation operator $\sigma_z x^2$. This mode can be excited by adding a spin-dependent trapping potential such that the two spin components experience different trapping frequencies. The normalized SB transition strength $\Gamma_n(\sigma x^2)$ is plotted in Fig. 1(d), and the mode frequency ω_{SB} across the whole phase diagram is plotted in Fig. 2 as circles with solid line. The behavior of ω_{SB} as a function of Ω is very simi-

lar to that of ω_{SD} we discussed above. As a result, we do not present a detailed discussion about this mode here.

VI. CONCLUSION

To summarize, we have presented detailed study of the collective excitation properties of a quasi-1D SO coupled BEC. This system possesses three phases which can be accessed by tuning the Raman coupling strength. We developed a method to efficiently classify the numerically obtained Bogoliubov excitation modes. We show that the dipole and the breathing modes become soft at the boundary between the PW and the ZM phases, but are smooth across the boundary between the ST and the PW phases. By contrast, the spin dipole and the spin breathing modes have distinct features in all three phases. We hope that our work may stimulate more experimental study of the collective excitation properties of SO coupled BEC.

Acknowledgments

L. Chen would like thank T.-T. Li for helpful discussion. YZ is supported by NSF of China under Grant Nos. 11234008 and 11474189, the National Basic Research Program of China (973 Program) under Grant No. 2011CB921601, Program for Changjiang Scholars and Innovative Research Team in University (PCSIRT)(No. IRT13076). ZQY is supported by NSFC under Grant No. 11674202. HP acknowledges support from US NSF and the Welch Foundation (Grant No. C-1669).

Appendix A: BOGOLIUBOV EQUATIONS AND NORMALIZED TRANSITION STRENGTH

In this Appendix, we provide more details on how the Bogoliubov spectrum and the normalized transition strength are calculated. The Bogoliubov equations are in the form of

$$\omega \mathbf{u} = (H_0 + A) \mathbf{u} + B \mathbf{v}, \quad (\text{A1})$$

$$-\omega \mathbf{v} = (H_0^* + A^*) \mathbf{v} + B^* \mathbf{u}, \quad (\text{A2})$$

where

$$A = \begin{pmatrix} 2g\rho_{0,\uparrow} + g_{\uparrow\downarrow}\rho_{0,\downarrow} - \mu & g_{\uparrow\downarrow}\psi_{0,\uparrow}\psi_{0,\downarrow}^* \\ g_{\uparrow\downarrow}\psi_{0,\uparrow}^*\psi_{0,\downarrow} & 2g\rho_{0,\downarrow} + g_{\uparrow\downarrow}\rho_{0,\uparrow} - \mu \end{pmatrix},$$

and

$$B = \begin{pmatrix} g\psi_{0,\uparrow}^2 & g_{\uparrow\downarrow}\psi_{0,\uparrow}\psi_{0,\downarrow} \\ g_{\uparrow\downarrow}\psi_{0,\uparrow}\psi_{0,\downarrow} & g\psi_{0,\downarrow}^2 \end{pmatrix},$$

are related to the two-body interaction, $\rho_{0,\sigma} = |\psi_{0,\sigma}|^2$ are the ground-state density, and μ denotes the chemical potential. In our numerical calculation, we first obtain the ground-state wave function Ψ_0 by propagating the Gross-Pitaevskii equations, Eq. (1) in the main text, in imaginary time. And then, the Bogoliubov spectrum ω_n as well as the amplitudes \mathbf{u}_n and \mathbf{v}_n can be worked out by directly diagonalize the Bogoliubov equations using the Arnoldi method [30].

In the framework of linear response theory, the total field operator $\hat{\Psi}$ can be linearized into the form of

$$\hat{\Psi}(x) = \Psi_0 + \sum_{n=1} \mathbf{u}_n \hat{b}_n + \mathbf{v}_n^* \hat{b}_n^\dagger, \quad (\text{A3})$$

where \hat{b}_n is the annihilation operator for the n th quasi-particle state $|n\rangle$. The transition strength $\Gamma_n(\hat{O})$ can be obtained by calculating the matrix element

$$\langle n|\hat{O}|0\rangle \equiv \int dx \langle n|(\hat{\Psi}^\dagger \hat{O} \hat{\Psi})|0\rangle.$$

Specifically, for the spin-independent operators $\hat{O} = x^{n'}$, we have

$$\langle n|x^{n'}|0\rangle = \int dx (\psi_{0,\uparrow} x^{n'} u_{n,\uparrow}^* + \psi_{0,\uparrow}^* x^{n'} v_{n,\uparrow}^* + \psi_{0,\downarrow} x^{n'} u_{n,\downarrow}^* + \psi_{0,\downarrow}^* x^{n'} v_{n,\downarrow}^*), \quad (\text{A4})$$

while for the spin-dependent operators $\hat{O} = \sigma_z x^{n'}$, we have

$$\langle n|\sigma_z x^{n'}|0\rangle = \int dx (\psi_{0,\uparrow} x^{n'} u_{n,\uparrow}^* + \psi_{0,\uparrow}^* x^{n'} v_{n,\uparrow}^* - \psi_{0,\downarrow} x^{n'} u_{n,\downarrow}^* - \psi_{0,\downarrow}^* x^{n'} v_{n,\downarrow}^*). \quad (\text{A5})$$

Again, we keep small amplitudes $\mathbf{u}_n(x)$ and $\mathbf{v}_n(x)$ into the linear term in Eqs. (A4) and (A5). Here $n' = 1$ and 2 correspond to the (spin) dipole and the (spin) breathing operators, respectively.

-
- [1] N. Goldman, G. Juzeliūnas, P. Öhberg, and I. B. Spielman, Rep. Prog. Phys. **77**, 126401 (2014).
- [2] H. Zhai, Rep. Prog. Phys. **78**, 026001 (2015).
- [3] Y.-J. Lin, K. Jiménez-García, and I. B. Spielman, Nature (London). **471**, 83 (2011).
- [4] P. Wang, Z.-Q. Yu, Z. Fu, J. Miao, L. Huang, S. Chai, H. Zhai, and J. Zhang, Phys. Rev. Lett. **109**, 095301 (2012).
- [5] L. W. Cheuk, A. T. Sommer, Z. Hadzibabic, T. Yefsah, W. S. Bakr, and M. W. Zwierlein, Phys. Rev. Lett. **109**, 095302 (2012).
- [6] T.-L. Ho, and S. Zhang, Phys. Rev. Lett. **107**, 150403 (2011).
- [7] Y. Li, L. P. Pitaevskii, and S. Stringari, Phys. Rev. Lett. **108**, 225301 (2012).
- [8] Y. Li, G. I. Martone, L. P. Pitaevskii, and S. Stringari, Phys. Rev. Lett. **110**, 235302 (2013).
- [9] S.-C. Ji, J.-Y. Zhang, L. Zhang, Z.-D. Du, W. Zheng, Y.-J. Deng, H. Zhai, S. Chen, and J.-W. Pan, Nature Phys. **10**, 314 (2014).
- [10] J. Li, J. Lee, W. Huang, S. Burchesky, B. Shteynas, F. C. Top, A. G. Jamison, and W. Ketterle, arXiv:1610.08194.
- [11] H. Hu, B. Ramachandhran, H. Pu, and X.-J. Liu, Phys. Rev. Lett. **108**, 010402 (2012); S. Sinha, R. Nath, and L. Santos, Phys. Rev. Lett. **107**, 270401 (2011).
- [12] ST phase has recently been directly observed in the experiment [10], where instead of the two hyperspin states, as we considered here, they used atoms trapped in a double well potential to represent the pseudo-spin degrees of freedom.
- [13] G. I. Martone, Y. Li, L. P. Pitaevskii, and S. Stringari, Phys. Rev. A **86**, 063621 (2012).
- [14] W. Zheng, Z.-Q. Yu, X. Cui, and H. Zhai, J. Phys. B **46**, 134007 (2013); S.-C. Ji, L. Zhang, X.-T. Xu, Z. Wu, Y. Deng, S. Chen, and J.-W. Pan, Phys. Rev. Lett. **114**, 105301 (2015).
- [15] Z. Chen, and H. Zhai, Phys. Rev. A **86**, 041604(R), (2012).
- [16] J.-Y. Zhang, S.-C. Ji, Z. Chen, L. Zhang, Z.-D. Du, B. Yan, G.-S. Pan, B. Zhao, Y.-J. Deng, H. Zhai, S. Chen, and J.-W. Pan, Phys. Rev. Lett. **109**, 115301 (2012).
- [17] Y. Li, G. I. Martone, and S. Stringari, Europhys. Lett. **99**, 56008, (2012).
- [18] S. Stringari, arXiv: 1609.04694.
- [19] C. Zhu, L. Dong, and H. Pu, J. Phys. B **49**, 145301 (2016).
- [20] X. Antoine and R. Duboscq, Comput. Phys. Commun. **185**, 2969 (2014).
- [21] L. P. Pitaevskii and S. Stringari Bose–Einstein Condensation (Oxford: Oxford Science) (2003).
- [22] The Gross-Pitaevskii-Bogoliubov theory for weakly-interacting Bose gas is valid when the quantum depletion (QD) is small. We have checked that QD is on the order of a few percent for the parameters we use in our calculation, and exhibits a peak at the PW and ZM boundary when $\Omega = \Omega_C^{P-Z}$, just as in the case of the 3D homogeneous system studied in the first paper of Ref. [14]. In the ST phase, QD remains negligible as long as the trap frequency is not too small. When the trap frequency approaches zero, the QD in the ST phase increases sharply with the nearly zero-energy mode making the dominant contribution. However, for a system in the thermodynamic limit, this mode corresponds to a Goldstone mode with exactly zero energy whose wave function is normalized as $\int dx(|\mathbf{u}|^2 - |\mathbf{v}|^2) = 0$, and should be excluded from the calculation of the QD.
- [23] S. Stringari, Phys. Rev. Lett. **77**, 2360 (1996).
- [24] T. Kimura, Phys. Rev. A **66**, 013608 (2002).
- [25] C. Menotti and S. Stringari, Phys. Rev. A **66**, 043610 (2002).
- [26] T. Bienaimé, E. Fava, G. Colzi, C. Mordini, S. Serafini, C. Qu, S. Stringari, G. Lamporesi, and G. Ferrari, Phys. Rev. A **94**, 063652 (2016).
- [27] A. Sartori, J. Marino, S. Stringari, and A. Recati, New J. Phys **17**, 093036, (2015).

- [28] W. Kohn, Phys. Rev. **123**, 1242 (1961); F. Dalfovo, S. Giorgini, L. P. Pitaevskii, and S. Stringari, Rev. Mod. Phys. **71**, 463 (1999).
- [29] X. Antoine, and R. Duboscq, Comput. Phys. Commun. **193**, 95 (2015).
- [30] W. E. Arnoldi, Q. Appl. Math. **9**, 17, (1951).